Available online at www.sciencedirect.com
SCIENCE DIRECT®
Journal of Nuclear Materials 328 (2004) 71–76
journal of nuclear materials
www.elsevier.com/locate/jnucmat

Letter to the Editors

A cubic-to-monoclinic structural transformation in the sesquioxide Dy_2O_3 induced by ion irradiation

M. Tang [a,b], J.A. Valdez [b], P. Lu [a], G.E. Gosnell [a,b], C.J. Wetteland [b], K.E. Sickafus [b,*]

[a] Department of Materials Science and Engineering, New Mexico Institute of Mining and Technology, Socorro, NM 87801, USA
[b] Materials Science and Technology Division, Los Alamos National Laboratory, Mail Stop G755, Los Alamos, NM 87545, USA

Received 22 July 2003; accepted 18 February 2004

Abstract

Polycrystalline pellets of the sesquioxide Dy_2O_3 were irradiated at cryogenic temperature with Kr^{++} ions to a fluence of 1×10^{20} Kr/m^2. The crystal structure of the irradiated Dy_2O_3 was observed to change from a cubic, so-called C-type rare-earth sesquioxide structure to a monoclinic, B-type rare-earth sesquioxide structure upon ion irradiation. This transformation is accompanied by a decrease in molecular volume (or density increase) of approximately 9%.

PACS: 61.80.Jh; 61.80.Ms; 61.16.Bg; 61.14.Lj; 61.10.Kw

1. Introduction

There has been considerable interest recently in the radiation damage behavior of oxides with structures related to fluorites, due to observations of impressive radiation tolerance in several different oxide compounds possessing the fluorite structure [1–3]. This letter addresses radiation damage evolution in Dy_2O_3 induced by Kr^{++} ion irradiation. Dy_2O_3 is a sesquioxide with the bixbyite crystal structure, a structure closely related to fluorite. Results presented here are compared to a previous study involving Xe^{++} ion irradiations of Dy_2O_3 [4].

Bixbyite is the mineral name for the cubic (α phase) polymorph of Mn_2O_3. Bixbyite belongs to space group $Ia\bar{3}$, with cations occupying 8*b* and 24*d* equipoints and anions occupying the 48*e* equipoint, so that there are 16 molecular units and 80 atoms per unit cell. The cations assume a face-centered cubic (*fcc*) arrangement, whilst the anions occupy tetrahedral interstices within this *fcc* cation lattice. [1] The tetrahedral interstices themselves form a simple cubic lattice, but only three-fourths of these sites are occupied by oxygen ions in a bixbyite crystal, due to the oxygen deficiency of an A_2O_3 bixbyite compared to a BO_2 fluorite (in the BO_2 fluorite, *all* tetrahedral interstices are occupied). The cations thus become sixfold coordinated by anions. In bixbyite, the empty sites on this pseudo-simple cubic anion sublattice are ordered so that the cubic unit cell is a super-cell, with twice the repeat unit of the cation sublattice (see Fig. 1). In Dy_2O_3, for instance, the cubic lattice parameter is $a = 1.06706(7)$ nm [5], while the cation sublattice repeat unit is only $a' = a/2 = 0.53353$ nm. In the study presented here, we will show that ion irradiation induces a

* Corresponding author. Tel.: +1-505 665 3457; fax: +1-505 667 6802.
E-mail address: kurt@lanl.gov (K.E. Sickafus).

[1] This description of the bixbyite is idealized to simplify the discussion. The cation sublattice is actually a distorted *fcc* lattice as the cations occupying the 24*d* equipoint are dilated by about 3% of a lattice unit from their ideal *fcc* positions (see, for example [5]).

0022-3115/$ - see front matter © 2004 Elsevier B.V. All rights reserved.
doi:10.1016/j.jnucmat.2004.02.014

transformation of Dy_2O_3 to a monoclinic, so-called B-rare-earth sesquioxide.

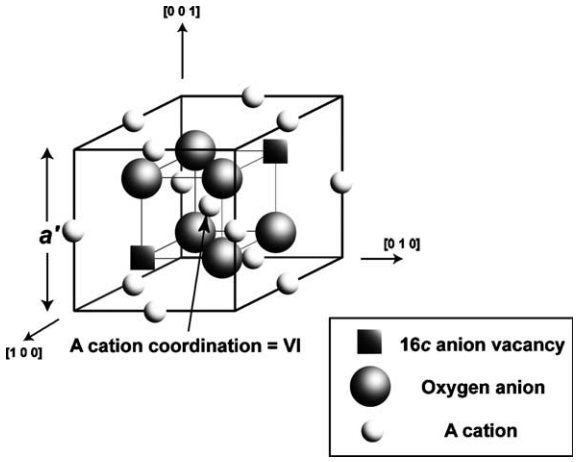

Fig. 1. One octant of an idealized A_2O_3 cubic bixbyite unit cell. The cations form an *fcc* arrangement, with anions in six of the eight available tetrahedral interstices. The vacant tetrahedral interstices (on the 16c equipoint) themselves form an ordered arrangement that causes the full unit cell to have twice the periodicity of this octant.

2. Experimental procedure

High purity Dy_2O_3 powders (Alfa Aesar 99.99% pure) were sintered at 1273 K for 24 h, then ball-milled and cold-pressed at a pressure of 6 metric tons. The green density of the pellets obtained by this procedure was ~75% of theoretical. Pellets were then calcined at 1273 K for 36 h, then sintered at 1923 K for 5 h, followed by 1773 K sintering for 36 h and slow cooling with the furnace off. The measured density of the final sintered product was 97% of theoretical. Using X-ray diffraction (XRD), the primary phase in the sintered pellets was determined to be consistent with the cubic bixbyite structure, with a lattice parameter given by $a = 1.065(4)$ nm (based on calibration using NIST #640c silicon powder standard reference material). The average grain size in the pellets was ~2 μm grain diameter (based on light and scanning electron microscopy observations). The pellets (13 mm diameter and lemon yellow in color) were cut into 0.5 mm thickness disks using a diamond saw and then polished with alumina lapping films to obtain a mirror finish.

Dy_2O_3 samples were irradiated with 300 keV Kr^{++} ions in the Ion Beam Materials Laboratory (IBML) at Los Alamos National Laboratory (LANL). Ion

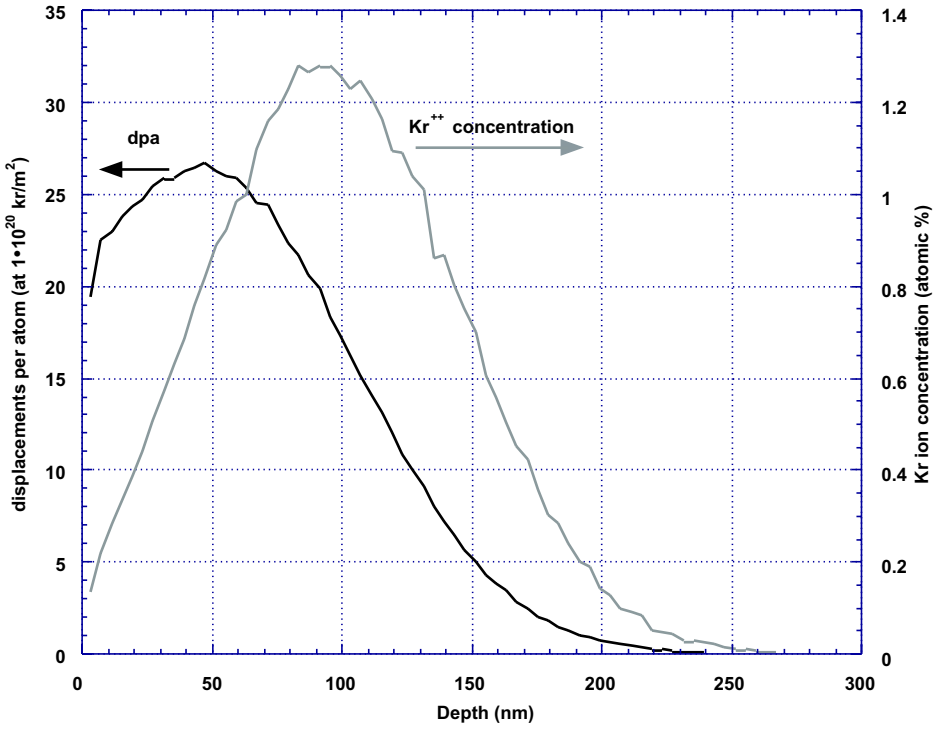

Fig. 2. Monte Carlo simulation results showing the displacement damage profile as a function of depth and the ion depth distribution for 300 keV Kr^{++} ion irradiation of cubic (C-phase) Dy_2O_3 to a fluence of 1×10^{20} Kr/m^2. The ion beam was oriented at normal incidence with respect to the sample substrate. The threshold for atomic displacements for both Dy and O were taken to be 40 eV in the calculations which is an arbitrary assumption.

implantations were performed at cryogenic temperature (~120 K) and at normal incidence using a dose rate of 2.8×10^{16} Kr^{++}/m^2 s to a fluence of 1×10^{20} Kr/m^2. The Monte Carlo program SRIM [6] was used to estimate the ion range profile and displacement damage distribution in the Dy_2O_3 substrate. Fig. 2 shows the results of this simulation. The peak in the displaced atom damage distribution occurs at a sample depth of 50 nm (corresponding to a peak displacement damage level of 25 displacements per atom (dpa) at fluence 1×10^{20} Kr/m^2), while the Kr ion range profile reaches maximum at a depth of 100 nm (corresponding to a peak implantation concentration of just over 1 at.% Kr at fluence 1×10^{20} Kr/m^2), with a longitudinal straggling of 50 nm.

Irradiated samples were then analyzed using either grazing-incidence X-ray diffraction (GIXRD) and transmission electron microscopy (TEM). GIXRD measurements were made using a Bruker AXS D8 Advanced X-ray diffractometer, Cu–K_α radiation, a graphite monochromator, θ–2θ geometry, and a fixed, 1° angle of incidence on the sample. The diffractometer was equipped with a Göebel mirror to achieve parallel beam diffraction optics. The θ–2θ scans were performed using a step size of 0.008° and a dwell time of 16 s per step. TEM observations were made using a Philips CM-30 instrument operating at 300 kV.

3. Results and discussion

Fig. 3 shows the results obtained using GIXRD on Dy_2O_3 before and after Kr^{++} ion irradiation to a fluence of 1×10^{20} Kr/m^2. GIXRD clearly reveals a change in structure of Dy_2O_3 at this radiation damage dose. The primary peaks in the unirradiated pattern at 29° and 33.6° are the {2 2 2} and {4 0 0} reflections from the cubic bixbyite phase of Dy_2O_3 (also known as the C-rare-earth sesquioxide structure). Following irradiation with Kr^{++} ions, the intensities of these cubic peaks are greatly diminished and new peaks emerge in the diffraction pattern. These new peaks are consistent with a monoclinic phase of Dy_2O_3 (JCPDF card 22-259 [7]). This phase was first observed in high temperature studies of rare-earth sesquioxides [8,9], and later in high pressure studies of the same sesquioxides [10–12]. This monoclinic phase is the so-called B-rare-earth

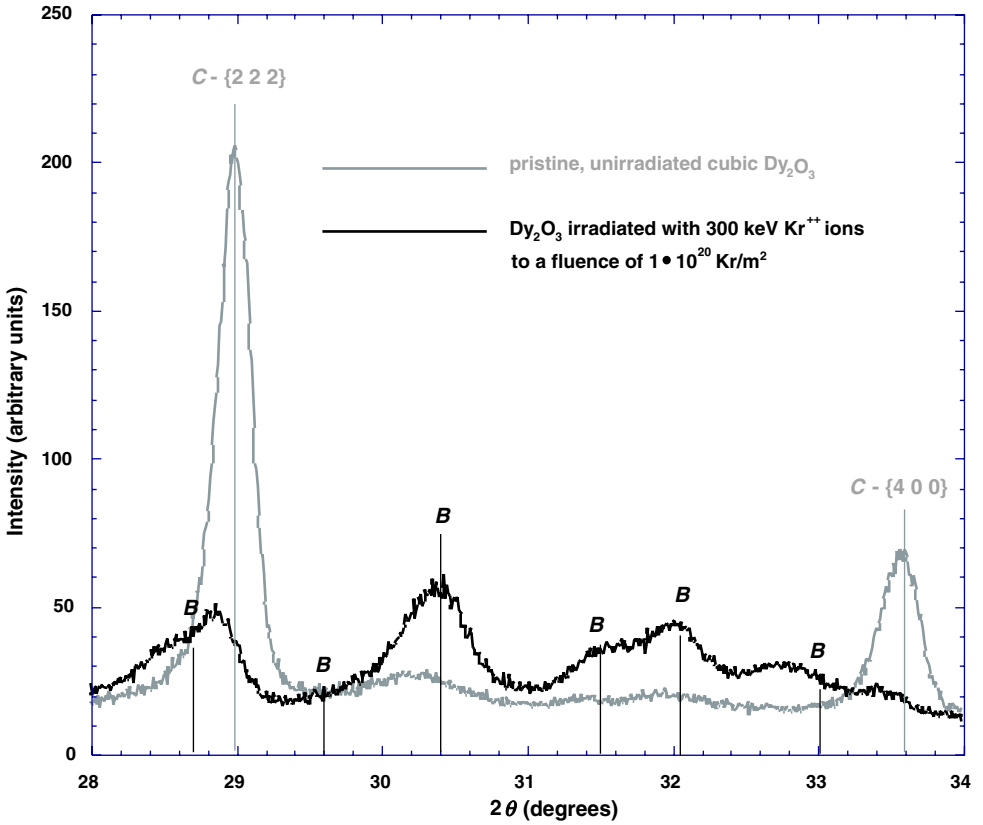

Fig. 3. GIXRD diffractometer scans obtained from pristine, unirradiated Dy_2O_3 (gray trace) and from a Dy_2O_3 substrate irradiated with 300 keV Kr^{++} ions to a fluence of 1×10^{20} Kr/m^2 (black trace). Scans were made at an X-ray incidence angle of 1°. Scans indicate a radiation-induced phase transformation from a cubic (C-type) to a monoclinic (B-type) sesquioxide structure.

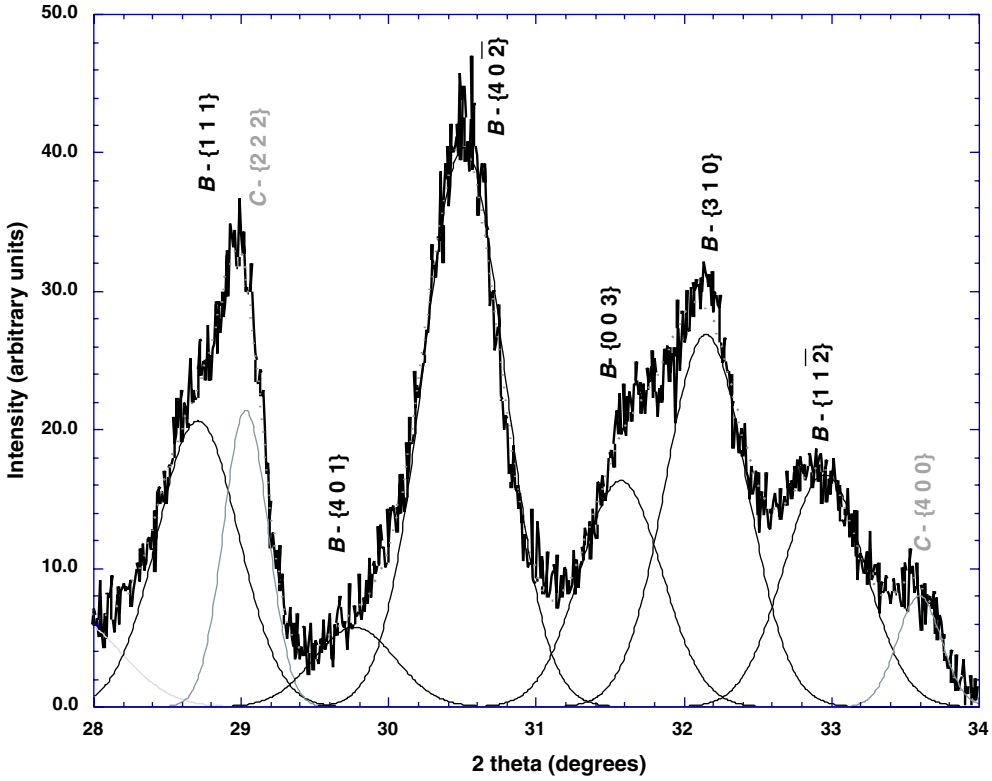

Fig. 4. Least square fit of Gaussian profiles to the diffraction maxima in the irradiated diffractometer scan from Fig. 3. The black trace is the measured diffraction data. The gray dotted trace is the sum of the Gaussian profiles used to fit the measured data. The peaks are identified with both B and C-type Dy_2O_3 and are indexed accordingly. The peak widths at half maximum are 0.3° for the cubic (C-type) peaks and 0.55° for the monoclinic (B-type) peaks. This difference is likely due to both strain and particle size broadening (the latter suggesting that the grain size in the implanted layer is significantly reduced compared to in the bulk).

sesquioxide structure and has been assigned to space group $C\,2/m$ (S.G. #12) [10].

Fig. 4 shows the results of a Gaussian-curve-fitting analysis of the Kr^{++}-ion-irradiated Dy_2O_3 GIXRD data presented in Fig. 3. Indexing of the reflections in Fig. 4 assumes that the new, irradiation-induced phase of Dy_2O_3 has a unit cell with dimensions similar to B-type Dy_2O_3 published earlier [11]. Then, given that interplanar spacings $d(hkl)$ in monoclinic structures are related to lattice parameters a, b, c, and β by

$$\frac{1}{d^2} = \frac{1}{a^2}\frac{h^2}{\sin^2\beta} + \frac{1}{b^2}k^2 + \frac{1}{c^2}\frac{l^2}{\sin^2\beta} - \frac{2hl\cos\beta}{ac\sin^2\beta} \qquad (1)$$

a least squares minimization procedure using the centroid positions of the Gaussians associated with the new monoclinic phase in Fig. 4, revealed that the radiation-induced monoclinic phase is characterized by lattice parameters $a = 1.390(8)$ nm, $b = 0.3504(2)$ nm, $c = 0.8624(7)$ nm, and $\beta = 100.06°$.

Fig. 5 shows results of cross-sectional transmission electron microscope (XTEM) observations of the microstructure associated with the Kr^{++} ion irradiated Dy_2O_3 samples. The micrographs show both bright-field (BF) and dark-field (DF) views of the implanted layer. The DF micrograph clearly shows that the grain size in the implanted layer is greatly diminished compared to the substrate (order of 80 nm diameter grains). Also, the DF image reveals that many of the grains possess orientation relationships with the unirradiated substrate (i.e., when the substrate is oriented in a Bragg diffraction condition, some implanted layer grains are simultaneously aligned for Bragg diffraction). This will be discussed further in a future report. Fig. 5 also shows microdiffraction (μD) patterns obtained from both the substrate (labeled 1) and different regions of the implanted surface layer (labeled 2 and 3). The substrate μD pattern indexes as the cubic bixbyite phase of Dy_2O_3 with an electron beam orientation given by $\vec{\mathbf{B}} = [121]$. The μD patterns from the implanted layer are consistent with a monoclinic B-phase of Dy_2O_3 with beam orientations given by $\vec{\mathbf{B}} = [\bar{1}34]$ (labeled 2) and $\vec{\mathbf{B}} = [\bar{1}32]$ (labeled 3). The $\vec{\mathbf{B}} = [\bar{1}34]$ μD pattern is the same as a

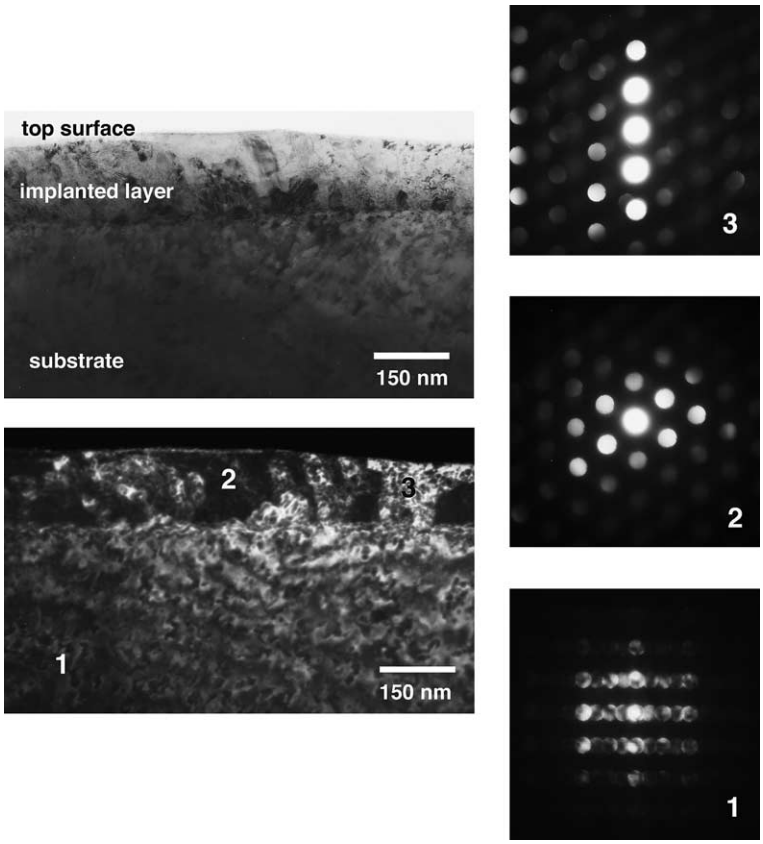

Fig. 5. XTEM results obtained from a Dy_2O_3 substrate irradiated with 300 keV Kr^{++} ions to a fluence of 1×10^{20} Kr/m^2. The top and bottom micrographs are BF and DF images, respectively. The μD patterns labeled 1–3 were obtained from regions labeled 1–3 in the DF image. The substrate μD pattern (labeled 1) indexes as the cubic bixbyite phase of Dy_2O_3 with $\vec{\mathbf{B}} = [1\,2\,1]$. The μD patterns from the implanted layer are consistent with a monoclinic B-phase of Dy_2O_3 with $\vec{\mathbf{B}} = [\bar{1}\,3\,4]$ (labeled 2) and $\vec{\mathbf{B}} = [\bar{1}\,3\,2]$ (labeled 3).

pattern published in our earlier study of Xe^{++} ion irradiated Dy_2O_3 [4], wherein the pattern was identified as coming from a disordered fluorite-structured Dy_2O_3 phase. The GIXRD and μD results presented here demonstrate clearly that the radiation-induced phase transformation in Dy_2O_3 is to a monoclinic B-type sesquioxide structure, not to a disordered fluorite phase.

The transformation for a cubic C-type to monoclinic B-type structure was observed previously in an ion irradiated sesquioxide. Specifically, Hémon et al. [13] irradiated Y_2O_3 with either 1 GeV Ta or 0.86 GeV Pb ions and observed a transformation from bixbyite structured Y_2O_3 (C-type) to monoclinic B or B1-type Y_2O_3. [2] Though the structural transformation in Y_2O_3 is identical to the transformation observed here for Dy_2O_3, the mechanisms must be very different, since the Y_2O_3 experiments were performed using primarily ionizing radiation, while predominately displacive radiation was employed in this study.

One interesting observation is that the density of the irradiation-induced B-phase is significantly greater than the unirradiated C-phase bixbyite. The volume per molecular unit was found to decrease upon irradiation from 0.0756 to 0.0690 nm^3/molecule, a decrease of nearly 9%. This result is similar to previous reports of volume contraction accompanying C- to B-transformations in sesquioxides (either temperature or pressure induced) (see, e.g. [10]). It should be noted that an increase in cation coordination is observed in the C- to B-transformation, from 6 in cubic bixbyite to a mixture of 6 and 7 in the monoclinic phase [16–18] (some authors describe cation coordination in the monoclinic phase as entirely sevenfold [11,19,20]). This cation coordination increase partly explains the increase in Dy_2O_3 density that accompanies the C–B transformation.

[2] B1 is a monoclinic phase, presumably structurally related to B, that has been observed in several previous examinations of polymorphism in rare earth sesquioxides (see for example [8,14,15]).

Explanations for this transformation are open to debate. Ion implantation can induce large near-surface compressive biaxial stress states (see, e.g., [21]), which in turn might lead to nucleation of a high-pressure phase such as the B-type Dy_2O_3 structure. But porosity in our Dy_2O_3 pellets (~3%) and the free surface associated with our implantation geometry, should conceivably assist stress relaxation and thereby mitigate pressure-induced phenomena. Displacive radiation damage can also cause materials to transform to higher-temperature polymorphs (see, for instance, irradiation effects in ZrO_2 [2]), suggesting that the irradiation-induced B-type Dy_2O_3 phase is rationalized because it is a structure ordinarily observed at high temperature. But the transformation from cubic bixbyite (C-Dy_2O_3) to monoclinic, B-type Dy_2O_3 is accompanied by a *reduction* in crystalline symmetry, which is not a typical observation. More significantly, we observe the density of the irradiated Dy_2O_3 to increase significantly, whereas most materials irradiated under similar conditions show the opposite behavior (i.e., irradiation-induced swelling [22]). Experiments are now in progress to explore the irradiation-induced C- to B-transformation of Dy_2O_3 in more detail.

4. Summary

In conclusion, heavy ion irradiation of cubic C-type Dy_2O_3 leads to a radiation-induced crystal structure transformation to a monoclinic, B-type Dy_2O_3 phase. This transformation is accompanied by a 9% decrease in molecular volume (or an equivalent increase in atomic density). B-type Dy_2O_3 is both a high-temperature and a high-pressure rare-earth sesquioxide polymorph, and consequently, explanations for this transformation at present are merely speculative.

Acknowledgements

This work was sponsored by the Department of Energy, Office of Basic Energy Sciences, Division of Materials Sciences and Engineering.

References

[1] S.X. Wang, B.D. Begg, L.M. Wang, R.C. Ewing, W.J. Weber, K.V. Godivan Kutty, J. Mater. Res. 14 (12) (1999) 4470.
[2] K.E. Sickafus, H. Matzke, T. Hartmann, K. Yasuda, J.A. Valdez, P. Chodak III, M. Nastasi, R.A. Verrall, J. Nucl. Mater. 274 (1999) 66.
[3] K.E. Sickafus, L. Minervini, R.W. Grimes, J.A. Valdez, M. Ishimaru, F. Li, K.J. McClellan, T. Hartmann, Science 289 (2000) 748.
[4] K.E. Sickafus, J.A. Valdez, J.R. Williams, R.W. Grimes, H.T. Hawkins, Nucl. Instrum. and Meth. B 191 (2002) 549.
[5] E.N. Maslen, V.A. Streltsov, N. Ishizawa, Acta Cryst. B 52 (1996) 414.
[6] J.F. Ziegler, J.P. Biersack, U. Littmark, The Stopping and Range of Ions in Solids, Pergamon Press, New York, 1985.
[7] International Centre for Diffraction Data, Powder Diffraction File, Joint Committee on Powder Diffraction Standards, Philadelphia, PA, 1974–present.
[8] V.M. Goldschmidt, F. Ulrich, T. Barth, Skrift. Nors. Vidensk.-Akad. Oslo I Mat. Naturv. Kl. 5 (1925) 5.
[9] V.M. Goldschmidt, T. Barth, G. Lunde, Skrift. Nors. Vidensk.-Akad. Oslo I Mat. Naturv. Kl. 7 (1925) 5.
[10] H.R. Hoekstra, K.A. Gingerich, Science 146 (3648) (1964) 1163.
[11] H.R. Hoekstra, Inorg. Chem. 5 (5) (1966) 754.
[12] H.A. Seck, F. Dachille, R. Roy, Inorg. Chem. 8 (1) (1969) 165.
[13] S. Hémon, V. Chailley, E. Dooryhée, C. Dufour, F. Gourbilleau, F. Levesque, E. Paumier, Nucl. Instrum. and Meth. B 122 (1997) 563.
[14] I. Warshaw, R. Roy, J. Phys. Chem. 65 (11) (1961) 2048.
[15] A.E. Solov'ena, Neorg. Mater. 21 (1985) 808.
[16] L. Eyring, in: K.A. Gschneidner Jr., E. LeRoy (Eds.), Handbook on the Physics and Chemistry of Rare Earths: Volume 3 – Non-Metallic Compounds – I, North-Holland, Amsterdam, 1979, p. 337.
[17] T. Atou, K. Kusaba, Y. Tsuchida, W. Utsumi, T. Yagi, Y. Syono, Mater. Res. Bull. 24 (1989) 1171.
[18] Y. Yokogawa, M. Yoshimura, S. Somiya, J. Mater. Sci. Lett. 10 (1991) 509.
[19] A.M. Lejus, R. Collongues, in: E. Kaldis (Eds.), Current Topics in Materials Science, vol. 4, 1980, p. 481.
[20] Y.J. Kim, W. Kriven, J. Mater. Res. 13 (10) (1998) 2920.
[21] A. Misra, S. Fayeulle, H. Kung, T.E. Mitchell, M. Nastasi, Nucl. Instrum. and Meth. B 148 (1999) 211.
[22] H. Matzke, Nucl. Instrum. and Meth. B 116 (1996) 121.